CONF-960608--5

DOE/MC/26041-96/C0683

Flow Interaction in the Combustor-Diffuser System of Industrial Gas Turbines

Author:

Agrawal, Kapat, Yang

Contractor:

Clemson University
216 EIB
Clemson, South Carolina 29634 - 0921

Contract Number:

DE-AC21-89MC26041

Conference Title:

American Society Mechanical Engineers, International Gas Turbine Institute

Conference Location:

Birmingham, UK

Conference Dates:

June 10-13, 1996

Conference Sponsor:

American Society of Mechanical Engineers

Contracting Officer Representative (COR):

Leland Paulson, D06

DISCLAIMER

DISCLAIMER

FLOW INTERACTIONS IN THE COMBUSTOR-DIFFUSER SYSTEM OF INDUSTRIAL GAS TURBINES[1]

Ajay K. Agrawal
School of Aerospace and Mechanical Engineering
University of Oklahoma, Norman, Oklahoma

Jayanta S. Kapat and Tah-teh Yang
Department of Mechanical Engineering
Clemson University, Clemson, South Carolina

ABSTRACT

This paper presents an experimental/computational study of cold flow in the combustor-diffuser system of industrial gas turbines to address issues relating to flow interactions and pressure losses in the pre- and dump diffusers. The present configuration with can annular combustors differs substantially from the aircraft engines which typically use a 360 degree annular combustor. Experiments were conducted in a one-third scale, annular 360-degree model using several can combustors equispaced around the turbine axis. A 3-D computational fluid dynamics analysis employing the multidomain procedure was performed to supplement the flow measurements. The measured data correlated well with the computations. The airflow in the dump diffuser adversely affected the prediffuser flow by causing it to accelerate in the outer region at the prediffuser exit. This phenomenon referred to as the sink-effect also caused a large fraction of the flow to bypass much of the dump diffuser and go directly from the prediffuser exit to the bypass air holes on the combustor casing, thereby, rendering the dump diffuser ineffective in diffusing the flow. The dump diffuser was occupied by a large recirculation region which dissipated the flow kinetic energy. Approximately 1.2 dynamic head at the prediffuser inlet was lost in the combustor-diffuser system; much of it in the dump diffuser where the fluid passed through the narrow gaps and pathways. Strong flow interactions in the combustor-diffuser system indicate the need for design modifications which could not be addressed by empirical correlations based on simple flow configurations.

INTRODUCTION

Gas turbine engines employ a combustor-diffuser system between the compressor discharge and combustor(s). In this system, the flow decelerates in a prediffuser to recover the flow kinetic energy and to minimize the downstream friction losses. The dump diffuser uniformly distributes air to the combustor(s) to maintain combustor performance, stability and durability. Designs of diffuser systems are based on empirical data from simple flow configurations (Sovran and Klomp, 1967). However, the limited validity of empirical correlations and the need to improve the efficiency of advanced gas turbines has prompted investigations which consider flow interactions owing to the geometric complexities of the combustor-diffuser system.

The combustor-diffuser system studied extensively are those of typical aircraft engines using an annular combustor extending 360 degrees around the turbine axis. The diffuser system in these engines feeds the compressed air to the combustor: the combustion air through a combustor dome, and the cooling and dilution air through inner and outer annular jackets around the combustor. One of the first experimental investigations of this configuration was undertaken by Fishenden and Stevens (1977) and Stevens et al. (1978) who found that the total pressure loss was minimum when the velocity profile at the prediffuser outlet was symmetrical. In recent years, experiments by Honami and Morioka (1990) and Srinivasan et al. (1990a, 1990b) included flow through the combustor dome. Carrotte et al. (1993) compared performance of dump and short-faired combustor-diffuser systems.

The experimental approach of identifying an optimum design is both costly and time consuming. Furthermore, the geometric complexities often limit the data that can be obtained reliably by experiments. These difficulties have created an interest in computational fluid dynamics to predict the combustor-diffuser flow

[1] This work was performed at Clemson University, Clemson, South Carolina

field. Koutmos and McGuirk (1989) modeled flow in the axisymmetric configuration tested by Fishenden and Stevens (1977) and found that their predictions were of sufficient accuracy for engineering purposes. Little and Manner (1993) reached a similar conclusion from their computational study of flow in the 2D plane and annular diffuser systems.

The studies reviewed above avoided geometric complexities of the combustor support struts, fuel nozzles, and the dilution and cooling ports on the combustor liner. Karki (1990) incorporated details of a practical system in a 3-D computational model to reveal strong effects of the support strut and fuel nozzles on the flow field. Adkins et al. (1992) used a combination of empirical data, simplified and detailed analyses, and model tests to develop, evaluate and qualify an annular combustor-diffuser with a 180-degree bend accompanied with air extraction for turbine blade cooling.

The combustor-diffuser system of power generating gas turbines considered in this study differs substantially from that of aircraft engines (see Figure 1). Power turbines typically use several can combustors (instead of an annular combustor) equispaced around the turbine axis. Each of these combustor cans is surrounded by a combustor casing which receives air from the dump diffuser and feeds it to the combustor can. Each combustor casing/can is supported by a strut extending into the lower part of the dump diffuser. A transition piece carries hot combustion products from the circular combustor can to an annular sector inlet of the gas turbine expander. The advanced gas turbines use an impingement-cooled transition piece wherein an impingement sleeve surrounds the transition piece. As shown in Figures 1 and 2a, a portion of the compressor discharge air enters through the holes on the sleeve impacting on the transition piece surface and then flows towards the combustor can/combustor casing through the gap between the sleeve and the transition piece. The remaining compressor discharge air reaches the combustor can through bypass holes on the combustor casing.

Details of flow distribution and frictional losses in combustor-diffuser systems of power turbines are presently lacking in the existing literature. This paper aims to fill this existing gap by providing the experimental data and computational results.

TECHNICAL APPROACH

Cold flow experiments were conducted in a subscale model of the combustor-diffuser system of a power generating gas turbine. A closely approximated 3-D computational fluid dynamic analysis was also performed to compare and to supplement the flow measurements. Subsequently, an integrated computational/experimental approach was used to describe the global flow field and to evaluate pressure losses in the flow system. The following sections provide details of the experimental and computational components of this study.

Experimental

Test Model. The test model shown in Figure 2 was a one-third scale representation of the gas turbine section between the compressor discharge and the turbine expander inlet. The test model included geometric details of the hot gas flow path to provide realistic flow conditions in the combustor-diffuser. The combustion or the heat transfer processes, however, were not simulated because this study focused on the cold airflow in the pre- and dump diffusers. The test model was a 360-degrees representation of the gas turbine instead of a circumferential sector model containing 3 or 4 combustor cans. Because of the presence of side walls, particularly in areas where flow has an adverse pressure gradient, a segmental test section could induce local flow separation causing the flow field of interest to undergo significant modifications. Figure 2(b) shows the cross-sectional view of the test model on an azimuthal plane after the prediffuser exit and highlights circumferential locations of the combustor can/transition piece and combustor casing/impingement sleeve assemblies, and the combustor support struts. The airflow path is depicted in Figure 2(a). The air entering the test model passed through an annular prediffuser before discharging into a dump diffuser. The prediffuser inlet height, H, was 0.05m, the annulus radius ratio at the inlet was 0.84, the prediffuser area ratio was 1.6 and the prediffuser length was 4.2 times the inlet height. The dump diffuser distributed a portion of the air through holes in the impingement sleeve to provide impingement cooling of the transition piece, and the remaining air through bypass holes in the combustor casing. All of the air eventually entered the combustor can through primary, secondary, dilution and cooling holes.

Flow System. Figure 3 shows layout of the suction-type wind-tunnel used to induce the desired airflow through the test model. The ambient air entered through a square bell mouth inlet lip, the filters, a 90-degree bend, and a honeycomb followed by transition sections which guided airflow to an annular flow developing section. A nose cone at the upstream end of the inner pipe of this 1m long flow developing section allowed a gradual transition of the airflow while sealing the inside of the inner pipe. The inner pipe of the flow developing section was rigidly and concentrically mounted inside the outer pipe by four airfoils at the inlet and four support rods at the exit. The exit of the flow developing section then attached to the inlet of the test model. The airflow exited the test section through the turbine inlet (labeled in Figure 2a) simulator and then discharged into a 1.2m long, 2.1m wide, and 1.6m high plenum which allowed access to the interior of the test section, necessary to install measurement probes and traverse systems. Plenum also isolated the test section from vibrations and oscillations of the suction fan located downstream. The suction fan was belt driven by a 150 kW, 3-phase motor, and it operated at a constant speed. The flow rate through the test model was regulated by a set of computer controlled louvers at the fan inlet. The maximum average axial velocity at the test section inlet was 50 m/s corresponding to a flow rate of 4 m^3/s. The wind-tunnel was approximately 10m long while the test model was about 0.76m long. The centerline of the tunnel was 1m above the floor.

Measurement Plan. Wall static pressure, total pressure and velocity profiles were measured to characterize the flow field in the pre- and dump diffusers. The pressure was measured with Kiel and pitot-static probes. A single-wire, hot-film anemometer measured the radial and axial components of the velocity. Figure 4 identifies 5 planes in the test model, A, B, C, D, and S, where detailed profiles were obtained. At the first 4 planes, measurements were taken at two circumferential locations. Each station is identified by 3 characters. The first character refers to the plane and the next 2 characters identify the circumferential location: BC stands for Between Combustors and BS stands for Between combustor

support Struts. Computer-controlled single-axis traverse systems were used to move probes during profile measurements. The only access to planes A, B, C, and D was from the inside of the prediffuser inner wall. Thus, the traverse system was mounted on a support (shown in Figure 4) secured coaxially inside the test section: one end at the junction of the test section and upstream flow developing section and the other end at the turbine inlet simulator inside the plenum.

Data Acquisition. The pressure was measured by a pressure scanning system, Scanivalve MSS-48C. Each of the two pressure transducers in MSS-48C (+/- 0.17 bar and +/- 0.34 bar) could accept up to 48 pressure inputs. For each pressure measurement, 20 readings were taken in 6 seconds at a sampling rate of 3.33 Hz. Fluctuations at high frequencies were filtered out by setting the low-pass filter of the Scanivalve signal conditioner to 1 Hz. Because the sampling frequency was more than twice the filter frequency, no unwanted aliasing could corrupt the measurements. Velocity was measured by a single-wire, hot-film probe at longitudinal planes where the circumferential velocity was zero. This was the key condition behind applicability of the single-wire, hot-film probe in measuring the other two velocity components: radial and axial. At each point of measurement, the voltage outputs from the same hot-film probe were measured for two different orientations. These two orientations were 90 degrees apart and were such that one of the two components was always normal to the wire and the other component was normal to the wire in one orientation (called normal orientation) and parallel to the wire in the other orientation (called tangential orientation). Figure 5 shows the hot-film in two different orientations. The hot-film was calibrated in a blowing type wind-tunnel for the two different orientations. These calibrations provided relationships between (i) the voltage output and effective cooling velocity, and (ii) the yaw coefficient and tangential velocity. The axial and radial velocities could be derived from the hot-wire voltage outputs in normal and tangential orientations and the two calibration curves. The hot-wire operation was controlled by a TSI IFA-100 thermal anemometer and the voltage output was digitized by a Metrabyte DAS-20 board on a microcomputer.

Computational

A closely approximated 3-D computational fluid dynamic analysis was performed to supplement the measurements. Discrete combustor support struts and combustor casing/impingement sleeve assemblies disrupt the flow circumferentially: hence, the flow field is 3-D and it could not be simulated accurately by an axisymmetric analysis. In the circumferential direction, the exact same geometry of the combustor casing/impingement sleeve assembly (and the support strut) repeats cyclically. Additionally, each of these assemblies is symmetric about its midplane. Therefore, the computational domain in the circumferential direction extended to only one-half of the distance between two consecutive assemblies (or support struts) which was 1/28th of the full 360-degrees. Because of the geometric complexity, the computational region was divided into two subdomains. The lower domain consisted of the prediffuser and a portion of the dump diffuser directly facing the prediffuser. The upper domain included the remaining dump diffuser housing a combustor casing/impingement sleeve assembly. The support strut was split between the domains. These two domains shared an interface region through which boundary condition data were communicated and updated during computations.

Grid Generation. A structured grid was generated independently in each of the two domains. First, the computational domain was divided into subvolumes representing specific objects. The mesh was generated independently within each subvolume, which allowed local grid refinement and accurate representation of the flow obstructions. Figure 6 shows the body-fitted computational grid in the two domains at a longitudinal plane between the combustor support struts (also the midplane of the combustor casing/impingement sleeve assembly). The shaded grids in Figure 6 represent solid objects, such as the impingement sleeve and the transition piece. The computational grid in the lower domain consisted of 62,208 grids; 18 in the circumferential direction, 32 in the radial direction and 108 in the axial direction. A total of 63,648 grids were used in the upper domain; 18 in the circumferential direction, 52 in the radial and 68 in the axial direction.

Governing Equations and Boundary Conditions. Using Cartesian tensor notation, the governing equations for incompressible turbulent flow are expressed in the time-averaged form:

$$\frac{\partial(\rho V_j)}{\partial x_j} = 0 \qquad (1)$$

$$\frac{\partial(\rho V_j V_i)}{\partial x_j} = -\frac{\partial p}{\partial x_i} + \frac{\partial}{\partial x_j}\left(\mu_{eff}\frac{\partial V_i}{\partial x_j}\right) \qquad (2)$$

where $\mu_{eff}=\mu+\mu_t$ was the effective viscosity. The turbulent viscosity μ_t was obtained from the standard $\kappa-\epsilon$ model of turbulence. Because of the symmetry, the mass flow rate and the gradients of dependent variables were zero at the two cicumferential boundaries.

Inlet. In the lower domain, the axial velocity at the prediffuser inlet was prescribed from the measured data. Inlet radial and circumferential velocities were assumed zero. The inlet turbulence intensity was taken as 10% and the inlet turbulent energy dissipation was calculated from the inlet turbulence intensity. Inlet to the upper domain was the outlet of the lower domain in the interface region. Thus, the inlet conditions for the upper domain were taken and updated from the computed flow field in the lower domain.

Walls. The wall function approach for turbulent flows was employed. This approach requires that the logarithmic velocity profile bridge the region between a wall and a near wall node on the outside of the viscous sublayer. Turbulence in the near wall region was in local equilibrium.

Outlet. Because the combustion process was not simulated, the fluid exited the upper domain through the annular gap between the combustor can and combustor casing. The combustor can and the transition piece were impervious to the flow. A constant static pressure was specified at the outlet of the upper domain. The outlet of the lower domain was in the interface region. Computations in the lower domain required a prescription for pressure at the outlet which was taken (and updated) from computation in the upper

domain.

Solution Procedure. The governing equations for each dependent variable were integrated over the control volumes to result in the finite difference equations. Convection-diffusion terms in the governing equations were discretized using the upwind scheme. The sets of coupled non-linear equations were solved implicitly in an iterative manner. The computational steps to update boundary condition data at the interface of the domains are described as follows:

(1) Prescribe a pressure distribution at the outlet of the lower domain (or the interface).
(2) Compute flow field in the lower domain.
(3) Compute flow field in the upper domain. The flow solution in the lower domain provided inlet conditions for the upper domain.
(4) Return to step 2 with an updated pressure distribution at the interface obtained from the flow solution in the upper domain. Continue iterations until pressure distribution at the interface no longer changes.

It was necessary to underrelax changes in the pressure distribution at the interface. Underrelaxing avoided large differences between successive updates of pressure field at the interface which otherwise led to oscillations. An underrelaxation factor of 0.2 was found to be acceptable in this work. The computations proceeded serially on a single CPU. Thus, at the end of computations in a domain, the flow field data were saved on disk files before computations were initiated for the other domain. Each trial took approximately 120 flow iterations. The flow field calculated for an earlier trial served as the initial guess for the new trial. The overall flow field converged after 6 to 10 trials. Each trial took 12 to 15 CPU hours on a Sun Sparkstation 10 Model 30.

RESULTS and DISCUSSIONS

Comparison between Measurements and Computations. Figures 7 and 8 showing the axial velocity profiles at stations BBC and BBS in the prediffuser reflect a good agreement between measurements and computations. The velocity profiles at the two circumferential locations were nearly the same indicating that the flow was axisymmetric in this region. The axial velocity profiles at plane C are shown in Figures 9 and 10. The measured and computed axial velocity profiles correlated with each other at the two circumferential ports CBC and CBS. Plane C was at the prediffuser exit where the differences between axial velocity profiles at the two circumferential locations indicated that the flow was 3-D. The OD-peaked axial velocity profile at station CBS (Figure 10) indicated flow acceleration in the outer region of the prediffuser exit.

Figures 11 and 12 show, respectively, the velocity profiles at stations DBC and DBS in the lower dump diffuser. At station DBC, the computed and measured axial velocity profiles correlated well although the predicted values were smaller than the measured data. A possible explanation for this difference may be attributed to a misalignment of the combustor support strut. The axial velocity would be higher if the measurement plane did not coincide with the midplane of the support strut. Figure 12 shows excellent correlation between measurements and computations at station DBS. High negative axial velocities in the outer region of plane D suggest a sharp flow turning at the prediffuser exit. Finally, Figure 13 shows velocity profiles at station SBS which was parallel and underneath the interface of the computational domains (see Figure 4). The measured peak in the radial velocity was higher and narrower than predicted. Thus, the measurements showed a sharper flow turning at the prediffuser exit than the predictions. The computations and the measured data, however, exhibited the same flow features including a recirculation region underneath the impingement sleeve.

In this study, the measuring stations were assumed to have zero circumferential velocity. However, a slight misalignment in the test rig or probe orientation, and probe vibrations could introduce 3-D effects, and thus influence the measurements. In the present analysis, only one computational mesh was used. Thus, a check for grid size convergence with successively finer grids was not pursued. Considering the above limitations, the correlation reached between the measurements and computations is viewed as reasonable.

Prediffuser Wall Static Pressure Recovery. Figure 14 shows the measured and computed static pressure recovery coefficients, Cp $[=(p-p_a)/h_D]$ where p is the static pressure, 'a' refers to the prediffuser inlet, and h_D is the dynamic head at the prediffuser inlet. Experimental data and computed results along the inner and outer walls of the prediffuser show similar trends, although the measured static pressure recovery was lower. The pressure increased linearly along the inner wall of the prediffuser. At an axial distance of 3H from the prediffuser inlet the measured and computed Cp values were 0.35 and 0.45, respectively. An unusual observation was the decrease in the outer wall pressure at the prediffuser exit. This decrease was, however, consistent with the flow acceleration at station CBS evident in Figure 10.

Flow Field. General characteristics of the flow at the midplane of the combustor casing/impingement sleeve assembly (also in between the combustor support struts) are shown in Figure 15. Some of the velocity vectors in the lower domain are hidden at the interface because of the manual overlapping of the results from the two domains. Figure 15 identifies that the air in the prediffuser's outer region accelerated while exiting the prediffuser and then turned almost 180 degrees to reach the bypass holes on the combustor casing. This short-circuiting of the diffuser flow was identified as the sink effect of the combustor bypass holes (Yang, T-t., 1993). Because of the strong interactions in the pre- and dump diffuser flows, the prediffuser flow was far from being ideal. Flow acceleration in the prediffuser is undesirable to its performance because the primary function of the prediffuser is to decelerate the flow.

Another finding of this study was the recirculation region underneath the impingement sleeve, occupying nearly half of the distance between the prediffuser exit and the turbine inlet. Flow velocities in this recirculation region were comparable to those of the flow exiting the prediffuser. A recirculating flow dissipates the energy received from the main flow, thereby, contributing to the frictional losses. The flow also separated in the dump diffuser at the tip of the prediffuser's outer wall and in the space between the combustor casing and the prediffuser's outer wall. However, the size and strength of these eddies were relatively small. The velocity

vectors at the midplane of the support strut (also in between the combustor casing/impingement sleeve assembly) are shown in Figure 16. The flow in the pre- and dump diffusers was 3-D because the support strut completely blocked and redirected the prediffuser flow. The flow remained separated underneath the impingement sleeve near the turbine inlet.

Total Pressure Loss. The total pressure loss coefficients, λ_{ac}[=(Pa-Pc)/h_D ; where P is the mass-averaged total pressure, and 'a' and 'c' refer to the planes] were calculated using the total pressure profiles measured by the Kiel probe and the axial velocity profiles measured by the hot-film. The measured loss coefficient in the prediffuser was 0.02 at the longitudinal plane in between the combustors (ABC to CBC) and it was 0.12 at the longitudinal plane in between the struts (ABS to CBS). The measured loss coefficients were different at the two longitudinal planes because the mass flows at the prediffuser exit were different. A precise calculation of the total pressure loss coefficient would require detailed measurements at all circumferential locations. In the absence of such data, the loss coefficients presented above provided the upper and lower bounds. From 3-D computations the mass averaged total pressure loss coefficient in the prediffuser was 0.04 which was within the bounds established from measurements.

The measured loss coefficient in the lower dump diffuser at a longitudinal plane in between the struts (from station CBS to SBS) was 0.13. Because of the limited measurement locations, the loss coefficient could not be obtained at a plane in between the combustors. From 3-D computations the total pressure loss coefficient in the lower dump diffuser was 0.22. The total pressure loss coefficient could not be measured meaningfully in the upper portions of the dump diffuser. An upper bound on the loss coefficient was established from the total pressure measured in the stagnant annular space next to the combustor bypass holes. The total pressure at the bypass holes would strongly affect the mass-averaged total pressure in the upper dump diffuser because approximately two-third of the flow entered through the bypass holes. Based on this argument, the mass averaged pressure loss coefficient in the upper dump diffuser was 1.0. The corresponding value from 3-D computations was 0.93.

Table 1 summarizes the measured and computed pressure loss coefficients in the diffusers. Both the measurements and computations indicate that approximately 1.2 dynamic head at the prediffuser inlet (or the compressor discharge) was lost in the diffusers. Approximately 80% of this loss occurred in the upper dump diffuser where the fluid passed through the narrow gaps and pathways between combustor casing/impingement sleeve assemblies. The total pressure loss in the prediffuser was relatively small: only 3% of the total pressure loss in the diffusers. Yet, as a result of an ineffective prediffuser, the air would enter the dump diffuser at a high velocity and consequently would cause a much larger total pressure loss in the dump diffuser.

CONCLUSIONS

This study identified the flow field and pressure loss mechanisms in the combustor-diffuser system of industrial gas turbines. The bypass holes on the combustor casing exerted a strong influence on the pre- and dump diffuser flow fields. This was referred to as the sink-effect of the combustor bypass holes. The prediffuser outer flow accelerated and turned 180-degree while short-circuiting most of the dump diffuser. Thus, both the pre- and dump diffusers were ineffective in adequately diffusing the flow. Recirculation regions in the dump diffuser caused frictional losses by dissipating the flow kinetic energy. The total pressure loss could be minimized by a redesign of the prediffuser which avoided the sink effect. Similarly the configuration of the dump diffuser could be altered to reduce the extent of flow recirculation. The precise revisions necessary for the high system efficiency could be based on an optimization study. Clearly, the empirical correlations based on simple flow configurations are inadequate for such investigations.

ACKNOWLEDGMENTS

This work was performed under the Morgantown Energy Technology Center, Department of Energy contract number DE-AC21-89MC26041 and with assistance from Mr. Thomas Ekstrom at the General Electric Gas Turbine Technology Department, Schenectady, New York. Mr. Leland E. Paulson was the METC project manager.

REFERENCES

Adkins, R.C., Benin, A.C., Escher, P.C., Hellat, J., and Koenig, W.M., 1992, "A Combustor Diffuser of Annular Configuration Suitable for Industrial Gas Turbines," *ASME Paper 92-GT-41*.

Carrotte, J.F., Denman, P.A., Wray, A.P., and Fry, P., 1993, "Detailed Performance Comparison of a Dump and Short Faired Combustor Diffuser System," *ASME Paper 93-GT-331*.

Fishenden, C.R., and Stevens, S.J., 1977, "Performance of Annular Combustor-Dump Diffusers," *Journal of Aircraft*, vol. 14, pp. 60-67.

Honami, S., and Morioka, T., 1990, "Flow Behavior in a Dump Diffuser with Distorted Flow at the Inlet," *ASME Paper 90-GT-90*.

Karki, K.C., Oechsle, V.L., and Mongia, H.C., 1990, "A Computational Procedure for Diffuser-Combustor Flow Interaction Analysis," *ASME Paper 90-GT-35*.

Koutmas, P. and McGuirk, J.J., 1989, "Numerical Calculations of the Flow in Annular Combustor Dump Diffuser Geometries," *Proc Instn Mech Engrs, Part C*, vol 203, pp 319-331.

Little, A.R., and Manners, A.P., 1993, 'Predictions of the Pressure Losses in 2D and 3D Model Dump Diffusers," *ASME Paper 93-GT-184*.

Sovran, G., and Klomp, E.D., 1967, "Experimentally Determined Optimum Geometries for Rectilinear Diffusers with Rectangular, Conical or Annular Cross-Sections," in *Fluid Mechanics of Internal Flows*, Elsevier, New York.

Srinivasan, R., Freeman, W.G., Mozumdar, S., and Grahmann, J.W., 1990, "Measurements in an Annular Combustor-Diffuser System," *AIAA Paper 90-2162*.

Srinivasan, R., Freeman, W.G., Grahmann, J., and Coleman, E., 1990, "Parametric Evaluation of the Aerodynamic Performance of an Annular Combustor-Diffuser System," *AIAA Paper 90-2163*.

Stevens, S.J., Nayak, U.S.L., Preston, J.F., Robinson, P.J., and Scrivener, C.T.J., 1978, "Influence of Compressor Exit Conditions on Diffuser Performance," *Journal of Aircraft*, vol 15, pp. 482-488.

Yang, T-t, 1993, Private Communication with Morgantown Energy Technology Center, US Department of Energy.

Table 1. Total Pressure Loss Coefficients in the Combustor-Diffuser System

	Measurements	Computations
Prediffuser	0.02 to 0.12	0.04 (3%)
Lower Dump Diffuser (between struts only)	0.12	0.22 (19%)
Upper Dump Diffuser	< 1.0	0.93 (78%)
Total	< 1.20	1.19 (100%)

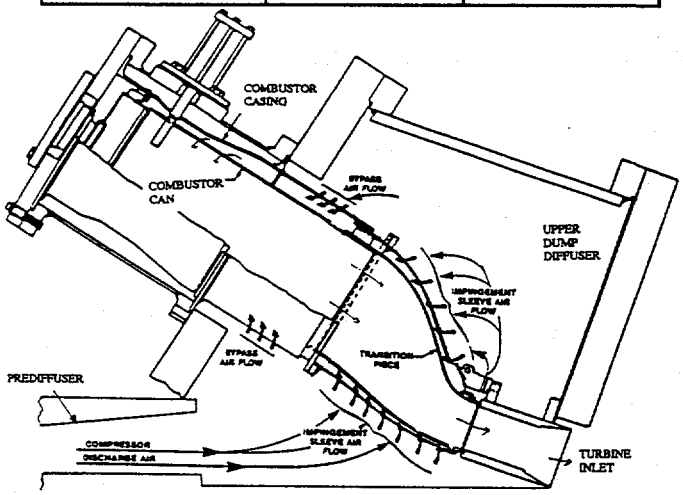

Figure 1. Combustor-Diffuser System of Typical Industrial Gas Turbines

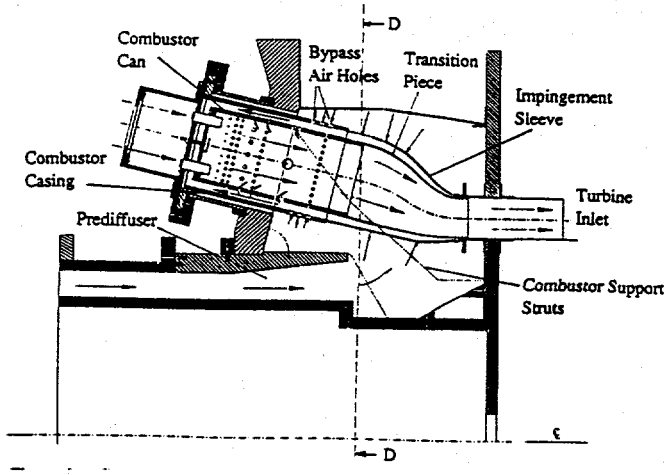

Figure 2a. Cross-sectional View of the Test Model; Longitudinal Plane in Between the Combustor Support Struts

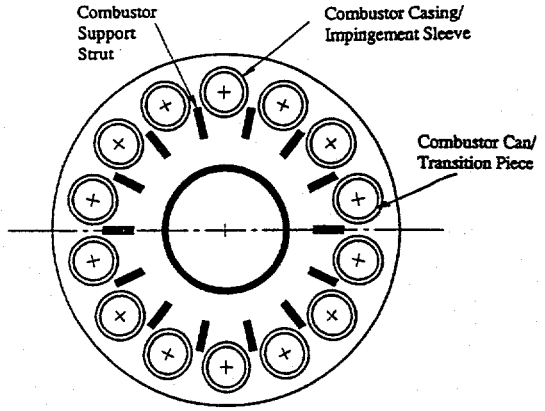

Figure 2b. Cross-sectional View of the Test Model; Azimuthal Plane at Section DD

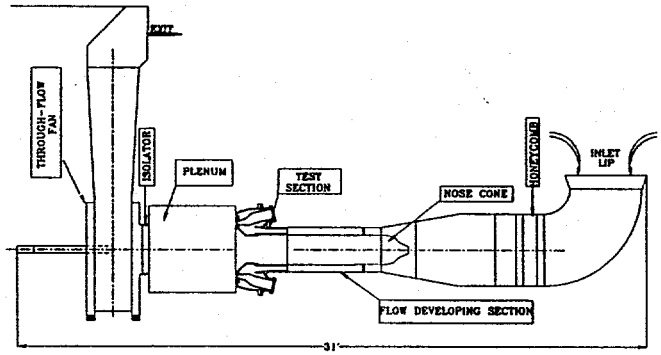

Figure 3. Layout of the Suction Type Wind-Tunnel

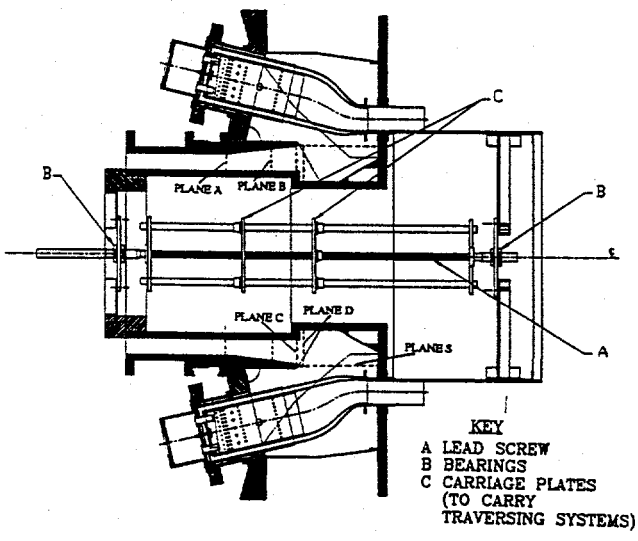

Figure 4. Measurement Locations and Schematic for Mounting the Traverse Support System

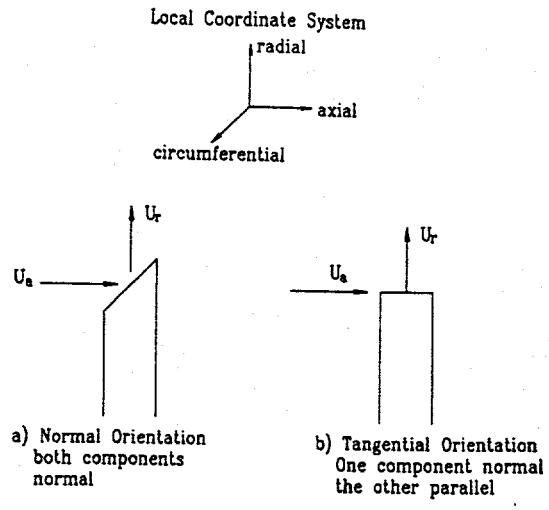

Figure 5. Two Orientations of a Single-Wire Hot-Film Probe

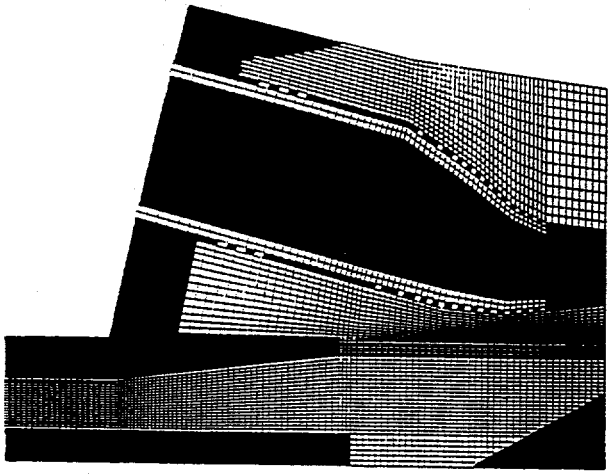

Figure 6. Computational Grid in the Two Domains; Longitudinal Plane in Between the Combustor Support Struts

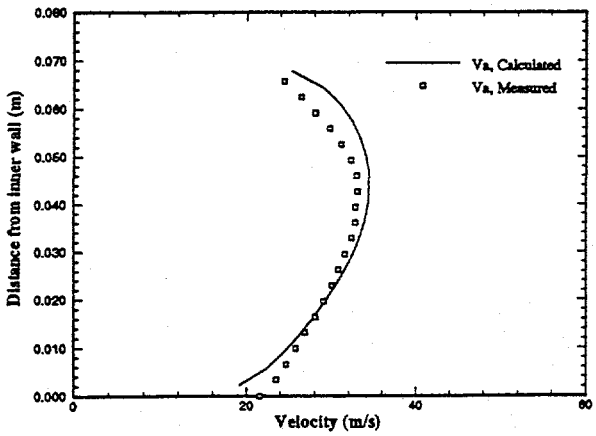

Figure 7. Axial Velocity Profiles at Station BBC

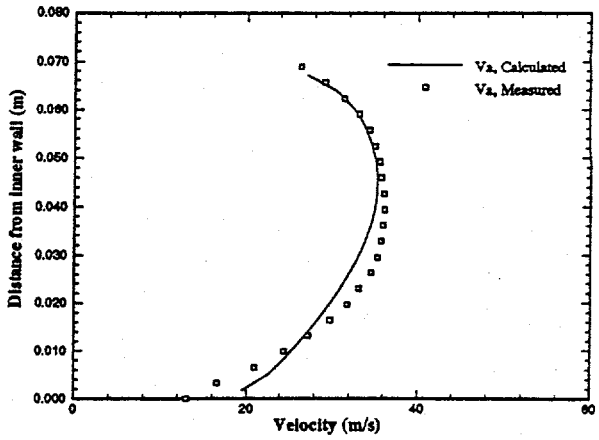

Figure 8. Axial Velocity Profiles at Station BBS

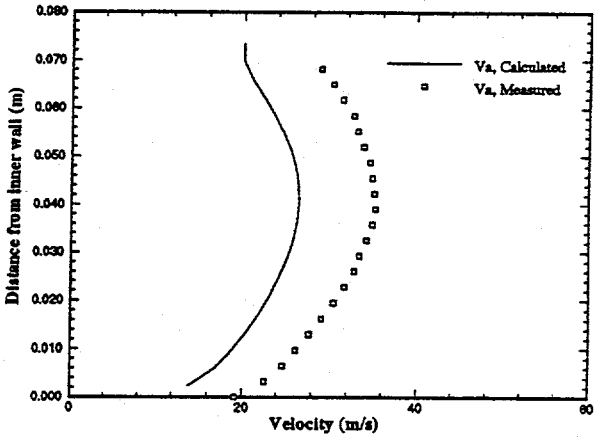

Figure 9. Axial Velocity Profiles at Station CBC

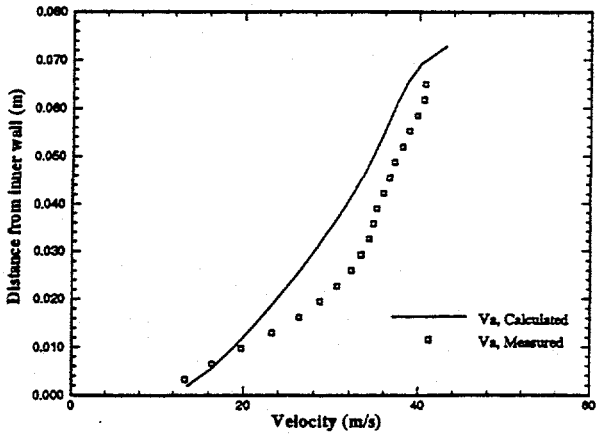

Figure 10. Axial Velocity Profiles at Station CBS

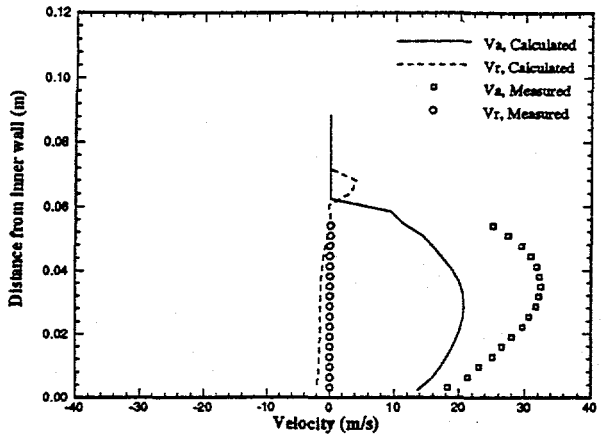

Figure 11. Velocity Profiles at Station DBC

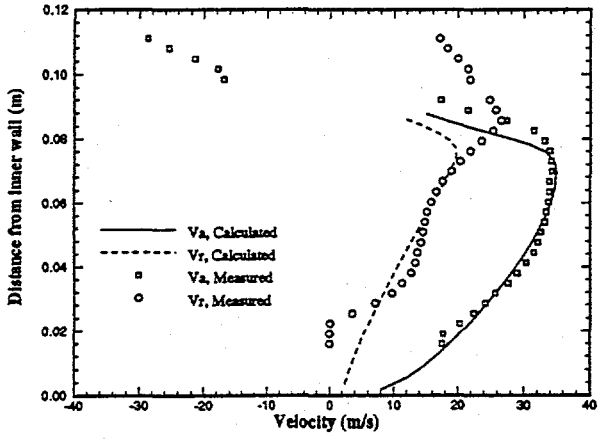

Figure 12. Velocity Profiles at Station DBS

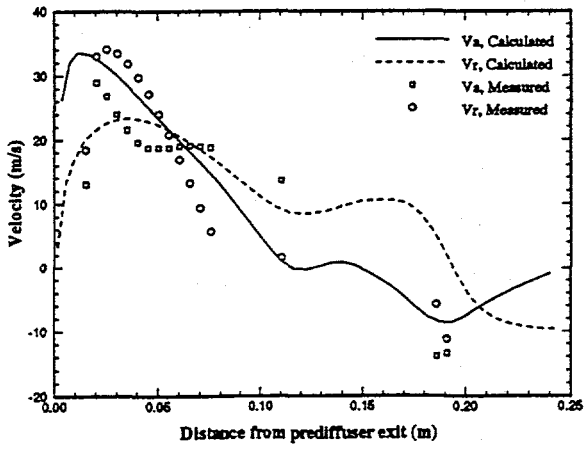

Figure 13. Velocity Profiles at Station SBS

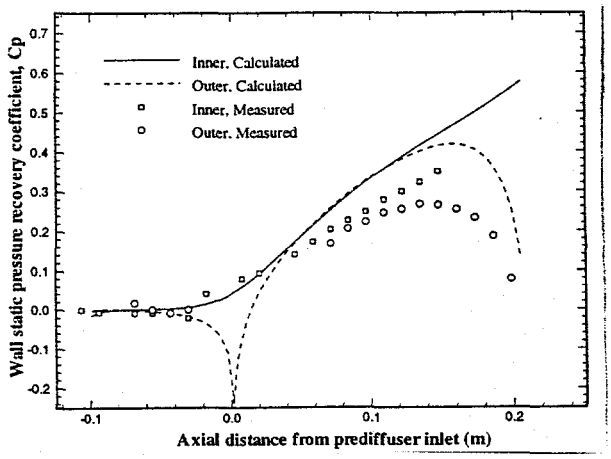

Figure 14. Prediffuser Wall Static Pressure Recovery Coefficient

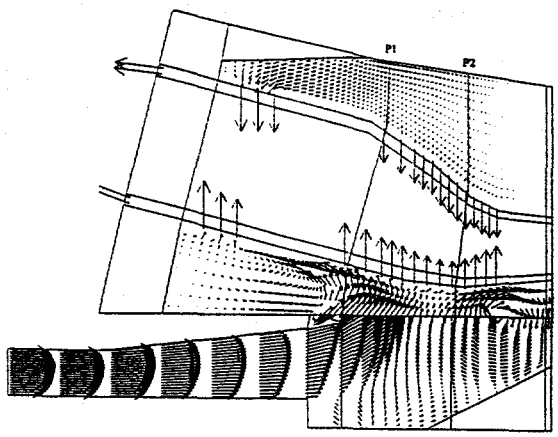

Figure 15. Velocity Vectors in the Diffusers; Longitudinal plane in Between the Combustor Support Struts

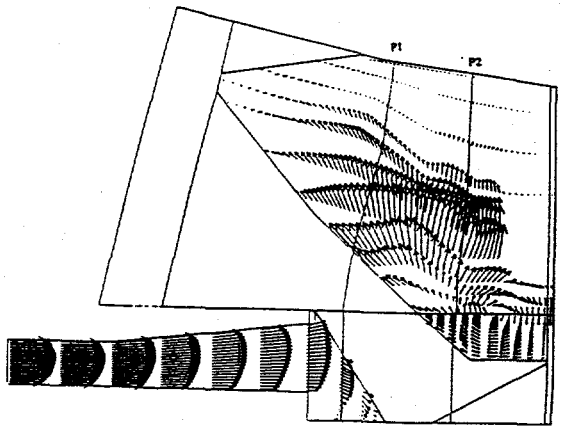

Figure 16. Velocity Vectors in the Diffusers; Longitudinal Plane in between the Combustor Casing/Impingement Sleeve